Title page

Title

Dynamic changes in the transcriptome of oocytes during adolescent-onset PCOS in mice

Du Danfeng[1,2#], Deng Ke[1,2#], Fan Dengxuan[1,2], Zhang Shuo[2,3], Xu Congjian[1,2*]

Author information

1. Du Danfeng[1,2#] **First author** Attending doctor
   ORCID: 0000-0002-0753-334X
   Email: 693468525@qq.com
2. Deng Ke[1,2] **Co-First author** Doctoral student
   ORCID: 0000-0002-4098-1144
   Email：20111250023@fudan.edu.cn
3. Fan Dengxuan[1,2] **Second author** Associate chief physician
   Email：dxfan16@fudan.edu.cn
4. Zhang Shuo[2,3] **Third author** MD
   Email: chnszhang@163.com
5. Xu Congjian[1,2*] **Corresponding author** Professor
   ORCID: 0000-0002-7954-5892
   Email: xucongjian@fudan.edu.cn

*Xu Congjian is the **Corresponding author** and the **Last author**

Du Danfeng is the **First author** and will handle correspondence at all stages of refereeing and publication

# Deng Ke contributed equally to this work and should be listed as **Co-first author**

Authorship Contribution

1. Du Danfeng (First Author): Methodology, Software, Investigation, Formal Analysis, Writing-Original Draft.
2. Deng Ke (Co-First author): Data Curation, Investigation, Formal Analysis, Writing-Original Draft.
3. Fan Dengxuan: Resources, Supervision.
4. Zhang Shuo: Resources, Supervision.
5. Xu Congjian (Corresponding Author): Conceptualization, Funding Acquisition, Resources, Supervision.

Affiliations

[1]Obstetrics & Gynecology Hospital, Fudan University, Shanghai, China

[2]Shanghai Key Laboratory of Female Reproductive Endocrine-Related Diseases, Shanghai, China

[3]Shanghai Ji Ai Genetics & IVF Institute, Obstetrics and Gynecology Hospital, Fudan University, Shanghai China

[1,2,3]Address: No.128, Shenyang Road, Yangpu District, Shanghai, China

Zip code: 200000

Running head

Transcriptome of oocytes in PCOS mouse

Keywords

Oocyte, RNA-seq, PCOS, adolescent, mouse model

Abstract

An adolescent-onset PCOS mouse model was established using dehydroepiandrosterone (DHEA) to explore temporal changes in the transcriptome of oocytes. Oocyte RNA sequencing was conducted using smart-seq technology. Genes with a similar expression trend over time were identified using trend analysis. Significant selected genes were those exhibiting an opposite trend in the DHEA group compared with the control group. KEGG pathway enrichment analysis and gene regulatory network diagrams were examined for signaling pathways to identify potential hub genes related to the pathogenesis of PCOS. Oocytes were collected at six consecutive time points during the modeling of PCOS in mice. Four main trends of gene expression were extracted, of which six combinations of Venn diagrams were generated. KEGG pathway analyses revealed that hub genes were mainly enriched in oxidative phosphorylation, cell cycle, P53 signaling pathway and related pathways. mtDNA coding subunits (mt-Nd1, 2, 3, and 6, mt-Co1 and 2), cytochrome oxidase (Cox8a, 7a2l, and 4i1), NADH-ubiquinone oxidoreductase (Ndufa1, 2 and 6, Ndufb 9), and Uqcrq were markedly up-regulated in the DHEA group. Cell cycle-related genes (Skp1, Ccnb1, Orc1 and 5, Wee2, Mapk3, Cdc20) were abnormally down-regulated in the DHEA group. These genes may be potential candidates that have temporal actions in the pathogenesis of PCOS. This study provides a novel insight into the altered transcriptome of oocytes from PCOS mice and potential key genes that may play important roles in the development of PCOS.

Introduction

Polycystic ovarian syndrome (PCOS) is a common endocrine and metabolic dysfunction. Patients with PCOS may have an increased number of retrieved oocytes during IVF treatment, but the embryo cleavage rate is low for these patients (QIAO AND FENG 2011). Embryo developmental competence was reduced in a PCOS model induced by dehydroepiandrosterone (DHEA) (HUANG *et al.* 2015). The pathogenesis of PCOS is not fully elucidated, but some evidence indicates a strong heritable component in the development of PCOS. Several genome-wide association studies have identified approximately 200 candidate genes related to the risk of PCOS (CRESPO *et al.* 2018), but not a single fully penetrant variant gene has been reported to date. All candidate genes or mutations show a low penetrance associated with many other covariant factors, such as hormones, environmental changes or lifestyles (KHAN *et al.* 2019).

Considerable work has been done to classify PCOS in the last several decades, but the consensus regarding PCOS phenotypes remains controversial. Some researchers propose PCOS is mainly caused by ovarian-derived androgen excess, while others suggest it is a complex systemic metabolism disorder (LIZNEVA *et al.* 2016). Fetal exposure to excessive androgen, nutritional excess and hyperglycemia during critical stages of prenatal development may program neurobiological circuitry (MCCARTHY *et al.* 2018). Prenatally androgenized androgen receptor knockout mice and neuron-specific androgen receptor knockout mice did not develop PCOS-like symptoms (CALDWELL *et al.* 2017).

PCOS can be divided into adolescent- and adult-onset types according to the time of onset. During the pubertal maturation process of the hypothalamic-pituitary-ovarian axis, girls with a predisposition to PCOS may exhibit increased gonadotropin-releasing hormone and luteinizing hormone pulse frequencies, ultimately leading to an increased luteinizing hormone/follicle stimulating hormone ratio (ROTHENBERG *et al.* 2018). Some characteristics of PCOS, such as acne, irregular menses and polycystic ovary morphology, may also be normal physiological symptoms of puberty (WITCHEL *et al.* 2016). Puberty may activate the susceptibility to develop PCOS, which interferes with the normal pubertal transition. Other factors, such as elevated anti-Mullerian hormone secretion, luteinizing hormone secretion and

gonadotropin-releasing hormone pulse frequency, may disrupt the pubertal transition (WITCHEL AND PLANT 2020). Girls who do not establish a normal hypothalamic-pituitary-ovarian axis and mature along the PCOS trajectory may eventually develop persistent PCOS (PENA *et al.* 2020).

At present, the origin theory of PCOS is more inclined to the 'adolescence origin or developmental origin', in which adult-onset disease originates from maternal exposure and a high androgen environment or the abnormal establishment of hypothalamic-pituitary-ovarian axis feedback mechanisms in puberty. Refractory or medicine-resistant PCOS usually arises during puberty and is marked by insulin resistance, hyperinsulinemia and hyperandrogenism (OTTO-BUCZKOWSKA *et al.* 2018). Many polygenic genetic diseases may originate from maternal-derived abnormal genes in oocytes. Mouse models have long been used to study PCOS, yet despite many reports describing the reproductive and metabolic phenotype of PCOS mouse models, research on the oocyte itself remains sparse (CHAPPELL *et al.* 2020). The incidence rate of PCOS is low in women older than 35 years, and adult-onset PCOS is more likely to be self-limited with aging or relieved by medical treatment. Most of the cases with drug resistant or familial-like PCOS develop their symptoms from puberty, and may be described as having adolescent-onset PCOS. The latter may be the type of PCOS that should be given more attention in the research and clinical setting. The aim of this study was to investigate the dynamic temporal changes of the oocyte transcriptome during PCOS modeling. Transcriptome data at six consecutive time points during PCOS mouse modeling were analyzed to detect the dynamic trend of gene regulation and reveal critical genes or pathways that may be important candidate factors for PCOS development and further studies.

Materials and Methods

Construction of the adolescent onset PCOS mouse model

The prepubertal mouse was used to mimic the hyperandrogenic phenotype of patients with adolescent onset PCOS. Female ICR mice were purchased from Shanghai JieSiJie Laboratory Animal Co. [production license number: SCXK (Shanghai) 2018-0004, China] and housed at the laboratory animal center of Obstetrics and Gynecology Hospital of Fudan University. Mice were housed with free access to food and water, and a constant temperature, humidity and light duration. At 25 days of age, mice were subcutaneously injected with DHEA powder (MCE, HY-14650, China) (6 mg/100 g body weight/d) dissolved in corn oil (MCE, HY-1888,

China). All procedures were performed in accordance with the guidelines of Experimental Animals Management Regulations (version 2017-03-01, China).

Ovary morphology and serum testosterone measurement

Ovaries of mice from each group were removed quickly and fixed in 4% paraformaldehyde for morphological assessment. Five-μm sections of ovary tissue were mounted on glass slides and stained with hematoxylin and eosin. Ovary morphology was further examined under light microscopy. The day after the final DHEA injection, blood was collected and centrifugated at a speed of 1000×g for 10 min. Serum testosterone was measured using a mouse testosterone enzyme immunoassay kit (Westang Bio-tech Co., Ltd., F11580, China).

Oocyte collection

From 25 days of age to two weeks after the final DHEA injection, oocytes were collected every other week so that six time points were established (points 0–5, Figure 1). At each time point, a mouse from each group was selected randomly, one ovary was fixed in paraformaldehyde for morphology assessment, and the other ovary was punctured with a 1 ml syringe needle in HEPES (Sigma, 83264, USA) to collect germinal vesicle-stage oocytes. Granulosa cells were removed mechanically. Ten oocytes of the same size, translucent and in good condition, were selected from each group for RNA sequencing.

Transcriptome sequencing

The selected oocytes were processed for RNA extraction and reverse transcription within 1 h and were subjected to cDNA amplification and purification. Reverse transcription was performed using a SMARTer Ultra Low RNA Kit (Clontech, USA) directly in the cell lysate. Then, cDNA was amplified and purified using an Advantage 2 PCR Kit (Clontech). The cDNA library was sequenced using an Illumina sequencing platform (NovaSeq6000). The raw reads were cleaned by removing adaptor sequences, short sequences (length < 35 bp), low-quality bases (quality < 20) and ambiguous sequences. Hisat2 (version:2.0.4) was used to map the cleaned RNA-seq reads to the mouse mm10 genome with two mismatches, two gaps and one multi-hit allowed. The gene expression value was normalized by fragments per kilobase of exon per million mapped fragments (FPKM) and adjusted by a geometric algorithm.

Statistical Analysis

Data analysis was performed using the OmicShare tools, an open online platform

for bioinformatics analysis (https://www.omicshare.com/tools, China) (Figure 2). At each time point (Point 1–5), two group of genes were compared to identify differentially expressed genes (DEGs). To further investigate dynamic gene expression patterns during the modeling process, trend analysis was used to determine genes with the same expression trend over six consecutive time points in the control and DHEA groups. Genes with very small expression levels were considered to play a limited role in the development of the disease, so the raw data were filtered by removing genes with FPKM < 1. Data of four main trends were extracted from each group and used for further analysis. Genes with the same or different expression trends from each group were compared for overlaps and differences, and the results were visualized using Venn diagrams. Genes with different or contrary expression trends from the Venn diagrams were considered to be abnormal and were used for gene pathway enrichment analysis (Kyoto Encyclopedia of Genes and Genomes, KEGG) and gene regulatory network analysis to explore the function of these genes and pathways. Genes from the critical pathway of each gene regulatory network were listed as hub genes.

Results

Reproductive characteristics of PCOS mice

After three weeks of DHEA injection, the PCOS mouse model was successfully established (Figure 3A). Ovarian tissue histology showed large numbers of follicles at different stages of development in the control group, while ovaries in the PCOS group exhibited significantly increased cystic follicles with degenerate granulosa cell layers. Serum testosterone levels were significantly higher in the PCOS group versus healthy controls (Figure 3B). After the final DHEA injection, ovarian morphology gradually recovered to a normal state within 3 weeks (Figure 3C).

DEGs at different time points

Data from two groups were compared to identify genes up- or down-regulated in the DHEA group at each of the five time points examined (points 1–5). The top ten DEGs are listed below and ranked by Log2FC (Table 1-4).

Trend analysis

A total of 21,928 genes were identified in mouse oocytes, and 9,382 genes had FPKM > 1. Given that each gene had a different trend over time, data in each group was first analyzed through trend analysis to summarize genes with similar trends over time. Four main trends of data were selected for further analysis. In the control group,

249 analysis over six consecutive time points (points 0–5) showed 314 genes were
250 continuously up-regulated, 525 genes were continuously down-regulated, 717 genes
251 had a down-flat-up regulation trend and 859 genes had an up-flat-down regulation
252 trend (Figure 4A). In the PCOS group over the same time points, 1491 genes were
253 continuously up-regulated, 811 genes were continuously down-regulated, 1222 genes
254 showed a down-flat-up regulation trend and 334 genes showed an up-flat-down
255 regulation trend (Figure 4B).

256 **Venn diagram analysis**

257 Four selected trends of data were plotted as Venn diagrams to identify genes with
258 abnormal expression trends in the DHEA group. For genes with the same trend in
259 both groups, genes only expressed in the DHEA group were selected. For genes with a
260 contrary trend, overlapping genes of the two groups were selected. Six kinds of data
261 combinations and Venn diagrams were finally produced. Venn1 was produced with
262 genes expressed as 'trend1' in both the control and DHEA groups. In this diagram,
263 1372 genes were abnormally continuously up-regulated in the DHEA group (Figure
264 5B). Venn2 was produced with genes expressed as 'trend2' in both the control and
265 DHEA groups, with 743 genes abnormally down-regulated in the DHEA group
266 (Figure 6B). Venn3 was produced with genes expressed as 'trend1' in the control
267 group and genes expressed as 'trend2' in the DHEA group. Twenty genes were
268 abnormally down-regulated in the PCOS group (Figure 7B). Venn4 was produced
269 with genes expressed as 'trend2' in the control group and genes expressed as 'trend1'
270 in the DHEA group. Seventy-one genes were abnormally up-regulated in the DHEA
271 group (Figure 8B). Venn5 was produced with genes expressed as 'trend3' in both
272 groups, in which 967 genes were abnormally down-flat-up-regulated in the DHEA
273 group (Figure 9B). Venn6 was produced with genes expressed as 'trend4' in both
274 groups, in which 190 genes were abnormally up-flat-down-regulated in the PCOS
275 group (Figure 10B). The selected genes are marked with the red dotted circle.

276 **Genes clustering and KEGG analysis**

277 KEGG analysis was used to detect the biological functions of the above six
278 groups of selected genes. Genes abnormally up-regulated in the DHEA group were
279 mainly focused on oxidative phosphorylation, thermogenesis, and the Parkinson
280 disease pathway (Figure 5C). Genes abnormally down-regulated in the DHEA group
281 were mainly focused on the cell cycle pathway (Figure 6C). Genes abnormally
282 up-regulated in the control group but down-regulated in the DHEA group were mainly

283 focused on p53 signaling, PI3K-Akt, and glycolysis gluconeogenesis pathways
284 (Figure 7C). Genes down-regulated in the control group but up-regulated in the
285 DHEA group were mainly focused on oxidative phosphorylation, central carbon
286 metabolism in cancer, and the Alzheimer's disease pathway (Figure 8C). Genes
287 abnormally down-flat-up-regulated in the DHEA group were mainly focused on the
288 regulation of actin cytoskeleton pathway (Figure 9C). Genes abnormally
289 up-flat-down-regulated in the DHEA group were mainly focused on oxidative
290 phosphorylation, apoptosis and Huntington disease pathways (Figure 10C). The
291 above results suggested that the most important pathways were oxidative
292 phosphorylation and the cell cycle.

293 **Gene regulatory network and hub genes**

294 The selected genes from Venn diagrams were further investigated using gene
295 regulatory network analysis to define the weight of different pathways. The result
296 shows that pathways with the highest weight and strongest correlation were also
297 oxidative phosphorylation and the cell cycle (Figure 5-10D). Some representative
298 genes from a critical pathway were listed as potential hub genes (Table 5) and ranked
299 by FPKM. The most significant difference was focused on mitochondrial oxidative
300 phosphorylation. Hub genes abnormally up-regulated in the DHEA group included
301 mtDNA coding subunits (mt-Nd1, 2, 3, 6 and mt-Co1,2), cytochrome oxidase (Cox8a,
302 7a2l, and 4i1), NADH-ubiquinone oxidoreductase (Ndufa1, 2, 6; Ndufb 9), and Uqcrq.
303 Hub genes abnormally down-regulated in the DHEA group mainly focused on the cell
304 cycle, which included Skp1, Ccnb1, origin recognition complex (ORC) subunit 1, and
305 5, Wee2, Mapk3, and Cdc20. All the other specific genes are listed in the
306 supplementary documents (File1).

307 **Discussion**

308 This study performed transcriptome sequencing throughout the course of PCOS
309 development in a mouse model of adolescent PCOS to find the critical genes or
310 pathways that regulate oocyte growth and quality. Identified DEGs in oocytes from
311 the PCOS model were mainly focused on oxidative phosphorylation and the cell
312 cycle.

313 Some mitochondria-related genes were abnormally and consistently up-regulated
314 in the PDHEA group, even after the DHEA injection regime was completed. Mt-Nd-x
315 are key protein subunits of mitochondrial complex I, which is the main entrance for
316 electrons to the respiratory chain, and its dysfunction will lead to decreased ATP

production (FORMOSA *et al.* 2018). Mitochondrial complex I deficiency is associated with many clinical conditions, such as Leber hereditary optic neuropathy, mitochondrial encephalomyelopathy, and lactic acidosis (NG *et al.* 2020). Cytochrome c oxidase (COX) is the terminal enzyme of electron transport chains in mitochondria, and COX8a is required for maintenance of the structural stability of COX monomers and dimers (ROTKO *et al.* 2021). COX7a2l is one of the three COX7a subunits, responsible for organization of the mitochondrial respiratory chain and preventing metabolic exhaustion (FERNANDEZ-VIZARRA *et al.* 2022). Uqcrq is one of the ten nuclear genes encoding proteins of mitochondrial complex III, and mutations in Uqcrq are associated with a series of rare neuromuscular symptoms (BURSKA *et al.* 2021). NDUFA-x encodes accessory subunits of mitochondrial complex I, and deficiency of this complex is the most common defect of the oxidative phosphorylation system. Mutations in NDUFA2 cause leukoencephalopathy (PERRIER *et al.* 2018), and patients with Leigh syndrome were found to harbor a homozygous mutation in NDUFA1(HUTTULA *et al.* 2022) . Diseases caused by mitochondria deficiency may have some undetermined commonalities with PCOS, and the down regulation of mitochondrially encoded subunits of respiratory chain complexes may play an important role in the mitochondria dysfunction associated with PCOS (THOMPSON *et al.* 2020).

Mitochondrial dysfunction has been proven to be a vital factor of many cardiovascular diseases and also plays an important role in the pathogenesis of PCOS (PAPALOU *et al.* 2016). Mitochondria convert nutrients into energy and release reactive oxygen species, but high levels of reactive oxygen species cause damage to mitochondrial components or even induce apoptosis. Growing evidence indicates that patients with PCOS have an increased level of oxidative stress and decreased levels of antioxidants (SULAIMAN *et al.* 2018). The abnormal concentration of reactive oxygen species and antioxidant factors in follicular fluid from patients with PCOS may have adverse effects on oocyte quality, fertilization and embryo development (NUNEZ-CALONGE *et al.* 2016). mtDNA copy number is lower in women with PCOS and is negatively correlated with insulin resistance levels while positively associated with sex hormone-binding globulin levels (LEWIS *et al.* 2010). However, some studies suggested that mtDNA number was increased in patients with PCOS and this increase was regarded as a feedback response compensating for mitochondrial dysfunction. These paradoxical results may reflect different stages of disease manifestation.

mtDNA copy number increases during the early stage of PCOS as a compensatory effect, but decreases with disease development as the mitochondria fail to sustain normal function (ZHANG *et al.* 2019).

The markedly down-regulated genes in the DHEA group mainly focused on cell cycle. S-phase Kinase-Associated Protein1 (SKP1) is a core component of the Skp, Cullin, F-box containing complex, an E3 ubiquitin ligase that participates in a variety of cellular processes (THOMPSON *et al.* 2022). It was reported that reduced SKP1 expression induced chromosomal instability in both benign and malignant tumors (LEPAGE *et al.* 2021). Furthermore, SKP1 maintained synapsis in meiosis of both sexes (GUAN *et al.* 2020), and also affected the balance of epigenetic regulation (SHEN AND SPRUCK 2017). ORC proteins can bind DNA replication origins to initiate DNA synthesis, and ORC is especially important in controlling centriole and centrosome copy number (ORTEGA *et al.* 2016). Wee2 is an important oocyte-specific kinase, and its downregulation in oocytes resulted in high maturation-promoting factor activity and failure to mature to the meiosis-II stage (SANG *et al.* 2018). Cyclin B1 is responsible for the composition of maturation-promoting factor, and Ccnb1-null oocytes completed meiosis I but arrested at the meiotic interphase (LI *et al.* 2019). Dominant or recessive CDC20 mutations have been linked to adverse oocyte maturation, and may act as a potential molecular markers of oocyte/embryo quality (SANG *et al.* 2021). The relationship between all the hub genes mentioned above and PCOS has not been investigated until now. From these findings we propose that infertility or adverse pregnancy outcomes of patients with PCOS may result from mitochondrial dysfunction or abnormal meiotic regulation of oocytes.

Conclusion

This study provides a novel insight into differences in the transcriptomes of oocytes from control compared with PCOS mice. These findings could help focus on specific pathways or potential candidate genes that may play important roles during the development of adolescent onset PCOS.

Data Availability Statement

Raw data underlying this article will be available in Figshare (10.6084/m9.figshare.21516228). The authors affirm that all data necessary for confirming the conclusions of the article are present within the article, figures, and tables.

Acknowledgments

We thank Liwen Bianji (Edanz) (www.liwenbianji.cn/) for editing the English text of a draft of this manuscript.

Funding

This work was supported by funding from the National Natural Science Foundation of China to Xu Congjian (Grant number 82171639 and 82201807).

Statements and Declarations

Competing Interests: The authors have no competing interests to declare that are relevant to the content of this article.

Reference

Burska, D., L. Stiburek, J. Krizova, M. Vanisova, V. Martinek *et al.*, 2021 Homozygous missense mutation in UQCRC2 associated with severe encephalomyopathy, mitochondrial complex III assembly defect and activation of mitochondrial protein quality control. Biochim Biophys Acta Mol Basis Dis 1867**:** 166147.

Caldwell, A. S. L., M. C. Edwards, R. Desai, M. Jimenez, R. B. Gilchrist *et al.*, 2017 Neuroendocrine androgen action is a key extraovarian mediator in the development of polycystic ovary syndrome. Proc Natl Acad Sci U S A 114**:** E3334-E3343.

Chappell, N. R., B. Zhou, A. K. Schutt, W. E. Gibbons and C. S. Blesson, 2020 Prenatal androgen induced lean PCOS impairs mitochondria and mRNA profiles in oocytes. Endocr Connect.

Crespo, R. P., T. Bachega, B. B. Mendonca and L. G. Gomes, 2018 An update of genetic basis of PCOS pathogenesis. Arch Endocrinol Metab 62**:** 352-361.

Fernandez-Vizarra, E., S. Lopez-Calcerrada, A. Sierra-Magro, R. Perez-Perez, L. E. Formosa *et al.*, 2022 Two independent respiratory chains adapt OXPHOS performance to glycolytic switch. Cell Metab.

Formosa, L. E., M. G. Dibley, D. A. Stroud and M. T. Ryan, 2018 Building a complex complex: Assembly of mitochondrial respiratory chain complex I. Semin Cell Dev Biol 76**:** 154-162.

Guan, Y., N. A. Leu, J. Ma, L. Chmatal, G. Ruthel *et al.*, 2020 SKP1 drives the prophase I to metaphase I transition during male meiosis. Sci Adv 6**:** eaaz2129.

Huang, Y., Y. Yu, J. Gao, R. Li, C. Zhang *et al.*, 2015 Impaired oocyte quality induced by dehydroepiandrosterone is partially rescued by metformin treatment. PLoS One 10**:** e0122370.

Huttula, S., H. Vayrynen, S. Helisalmi, L. Kytovuori, L. Luukkainen *et al.*, 2022 NDUFA1 p.Gly32Arg variant in early-onset dementia. Neurobiol Aging 114**:** 113-116.

Khan, M. J., A. Ullah and S. Basit, 2019 Genetic Basis of Polycystic Ovary Syndrome (PCOS): Current Perspectives. Appl Clin Genet 12**:** 249-260.

Lepage, C. C., M. C. L. Palmer, A. C. Farrell, N. M. Neudorf, Z. Lichtensztejn *et al.*, 2021 Reduced SKP1 and CUL1 expression underlies increases in Cyclin E1 and chromosome instability in cellular precursors of high-grade serous ovarian cancer. Br J Cancer 124**:** 1699-1710.

Lewis, J. G., K. K. Borowski, B. I. Shand, P. M. George and R. S. Scott, 2010 Plasma sex hormone-binding globulin, corticosteroid-binding globulin, cortisol, and free cortisol levels in

outpatients attending a lipid disorders clinic: a cross-sectional study of 1137 subjects. Horm Metab Res 42: 274-279.

Li, J., W. P. Qian and Q. Y. Sun, 2019 Cyclins regulating oocyte meiotic cell cycle progressiondagger. Biol Reprod 101: 878-881.

Lizneva, D., L. Suturina, W. Walker, S. Brakta, L. Gavrilova-Jordan *et al.*, 2016 Criteria, prevalence, and phenotypes of polycystic ovary syndrome. Fertil Steril 106: 6-15.

McCarthy, M. M., K. Herold and S. L. Stockman, 2018 Fast, furious and enduring: Sensitive versus critical periods in sexual differentiation of the brain. Physiol Behav 187: 13-19.

Ng, Y. S., K. Thompson, D. Loher, S. Hopton, G. Falkous *et al.*, 2020 Novel MT-ND Gene Variants Causing Adult-Onset Mitochondrial Disease and Isolated Complex I Deficiency. Front Genet 11: 24.

Nunez-Calonge, R., S. Cortes, L. M. Gutierrez Gonzalez, R. Kireev, E. Vara *et al.*, 2016 Oxidative stress in follicular fluid of young women with low response compared with fertile oocyte donors. Reprod Biomed Online 32: 446-456.

Ortega, M. A., H. Nguyen and W. S. Ward, 2016 ORC proteins in the mammalian zygote. Cell Tissue Res 363: 195-200.

Otto-Buczkowska, E., K. Grzyb and N. Jainta, 2018 Polycystic ovary syndrome (PCOS) and the accompanying disorders of glucose homeostasis among girls at the time of puberty. Pediatr Endocrinol Diabetes Metab 24: 40-44.

Papalou, O., V. M. Victor and E. Diamanti-Kandarakis, 2016 Oxidative Stress in Polycystic Ovary Syndrome. Curr Pharm Des 22: 2709-2722.

Pena, A. S., S. F. Witchel, K. M. Hoeger, S. E. Oberfield, M. G. Vogiatzi *et al.*, 2020 Adolescent polycystic ovary syndrome according to the international evidence-based guideline. BMC Med 18: 72.

Perrier, S., L. Gauquelin, M. Tetreault, L. T. Tran, N. Webb *et al.*, 2018 Recessive mutations in NDUFA2 cause mitochondrial leukoencephalopathy. Clin Genet 93: 396-400.

Qiao, J., and H. L. Feng, 2011 Extra- and intra-ovarian factors in polycystic ovary syndrome: impact on oocyte maturation and embryo developmental competence. Hum Reprod Update 17: 17-33.

Rothenberg, S. S., R. Beverley, E. Barnard, M. Baradaran-Shoraka and J. S. Sanfilippo, 2018 Polycystic ovary syndrome in adolescents. Best Pract Res Clin Obstet Gynaecol 48: 103-114.

Rotko, D., A. P. Kudin, G. Zsurka, B. Kulawiak, A. Szewczyk *et al.*, 2021 Molecular and Functional Effects of Loss of Cytochrome c Oxidase Subunit 8A. Biochemistry (Mosc) 86: 33-43.

Sang, Q., B. Li, Y. Kuang, X. Wang, Z. Zhang *et al.*, 2018 Homozygous Mutations in WEE2 Cause Fertilization Failure and Female Infertility. Am J Hum Genet 102: 649-657.

Sang, Q., Z. Zhou, J. Mu and L. Wang, 2021 Genetic factors as potential molecular markers of human oocyte and embryo quality. J Assist Reprod Genet 38: 993-1002.

Shen, J., and C. Spruck, 2017 F-box proteins in epigenetic regulation of cancer. Oncotarget 8: 110650-110655.

Sulaiman, M. A., Y. M. Al-Farsi, M. M. Al-Khaduri, J. Saleh and M. I. Waly, 2018 Polycystic ovarian syndrome is linked to increased oxidative stress in Omani women. Int J Womens Health 10: 763-771.

Thompson, L. L., A. K. Baergen, Z. Lichtensztejn and K. J. McManus, 2020 Reduced SKP1 Expression Induces Chromosome Instability through Aberrant Cyclin E1 Protein Turnover. Cancers (Basel) 12.

471 Thompson, L. L., K. A. Rutherford, C. C. Lepage and K. J. McManus, 2022 Aberrant SKP1 Expression:
472 Diverse Mechanisms Impacting Genome and Chromosome Stability. Front Cell Dev Biol 10**:**
473 859582.
474 Witchel, S. F., and T. M. Plant, 2020 Intertwined reproductive endocrinology: Puberty and polycystic
475 ovary syndrome. Curr Opin Endocr Metab Res 14**:** 127-136.
476 Witchel, S. F., H. Roumimper and S. Oberfield, 2016 Polycystic Ovary Syndrome in Adolescents.
477 Endocrinol Metab Clin North Am 45**:** 329-344.
478 Zhang, J., Y. Bao, X. Zhou and L. Zheng, 2019 Polycystic ovary syndrome and mitochondrial
479 dysfunction. Reprod Biol Endocrinol 17**:** 67.
480

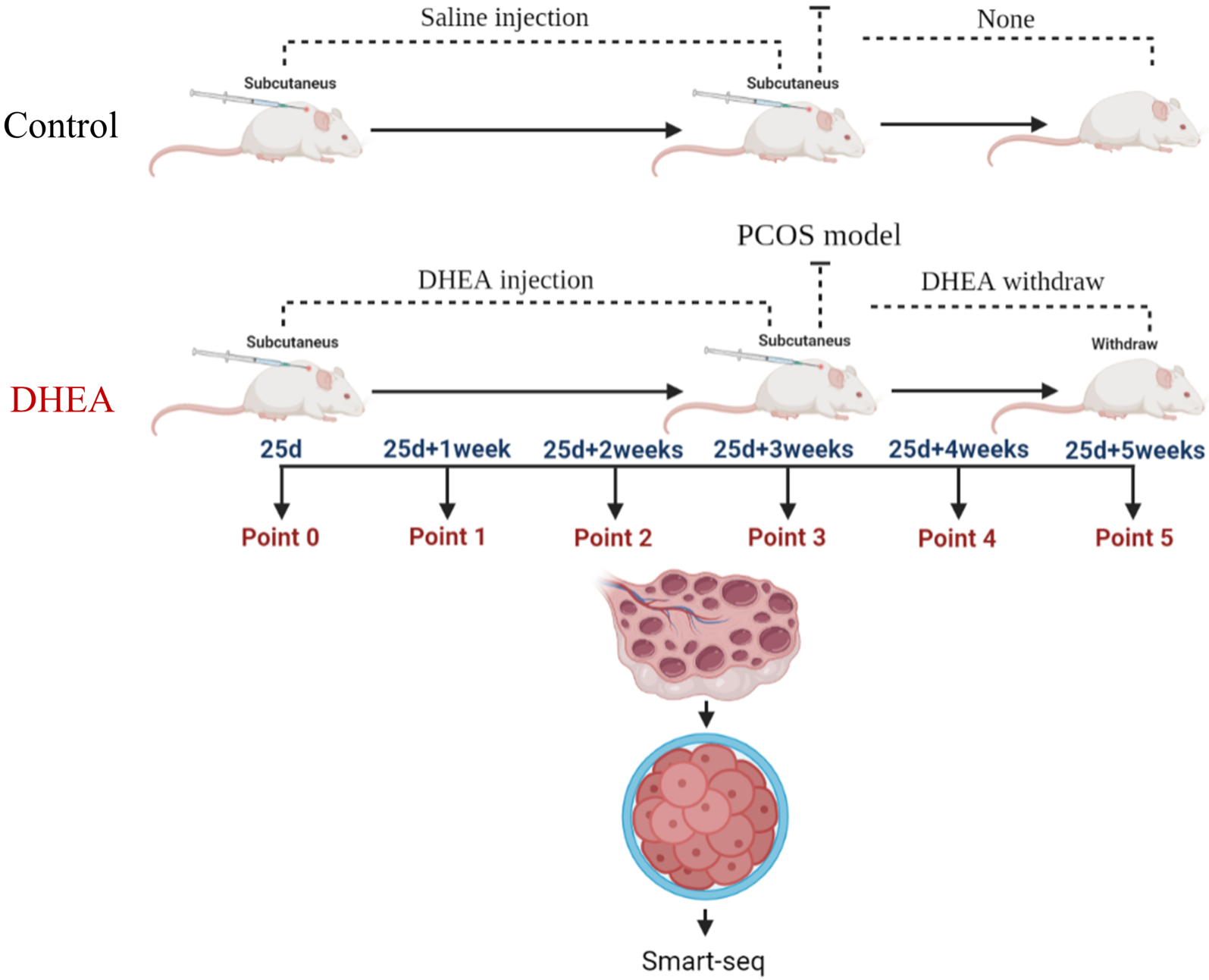
Saline injection
None
Control
Subcutaneus
Subcutaneus
PCOS model
DHEA injection
DHEA withdraw
DHEA
Subcutaneus
Subcutaneus
Withdraw
25d
25d+1week
25d+2weeks
25d+3weeks
25d+4weeks
25d+5weeks
Point 0
Point 1
Point 2
Point 3
Point 4
Point 5
Smart-seq

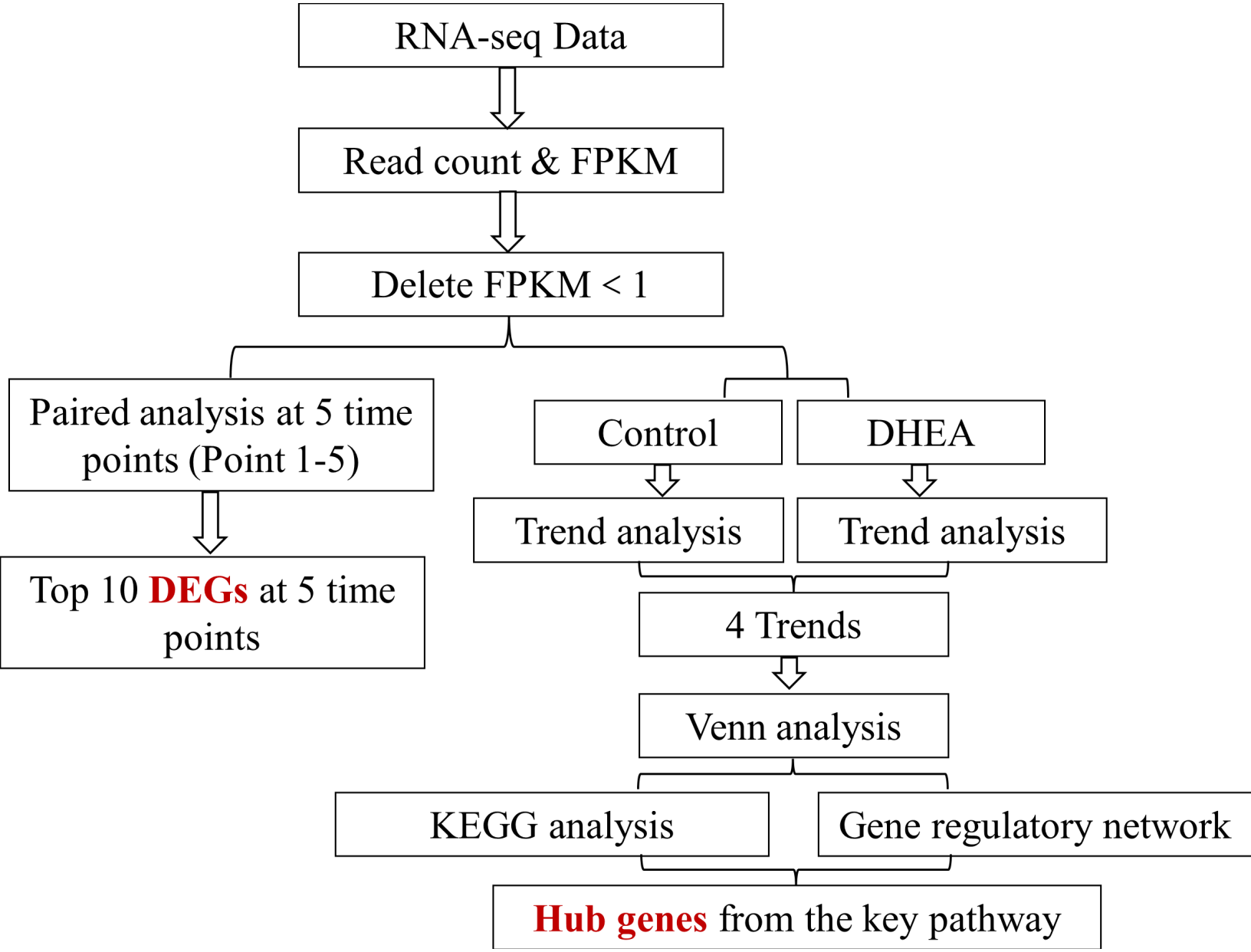
RNA-seq Data
Read count & FPKM
Delete FPKM < 1
Paired analysis at 5 time points (Point 1-5)
Top 10 DEGs at 5 time points
Control
DHEA
Trend analysis
Trend analysis
4 Trends
Venn analysis
KEGG analysis
Gene regulatory network
Hub genes from the key pathway

(A)

Control

PCOS

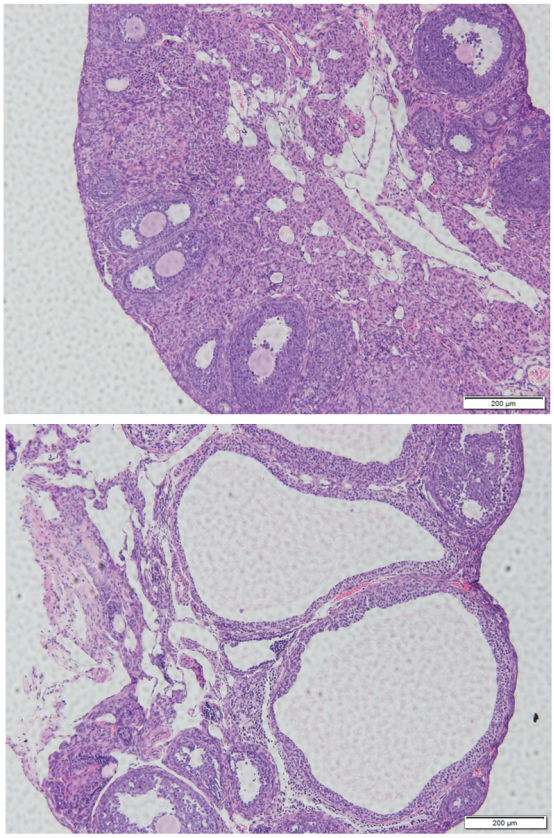

(B)

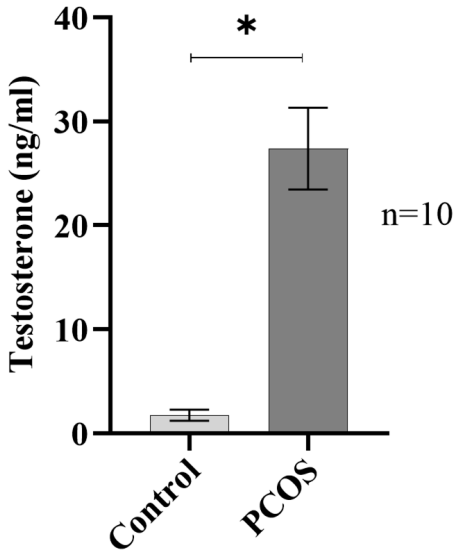

(C)

DHEA withdraw

1 week

2 weeks

3weeks

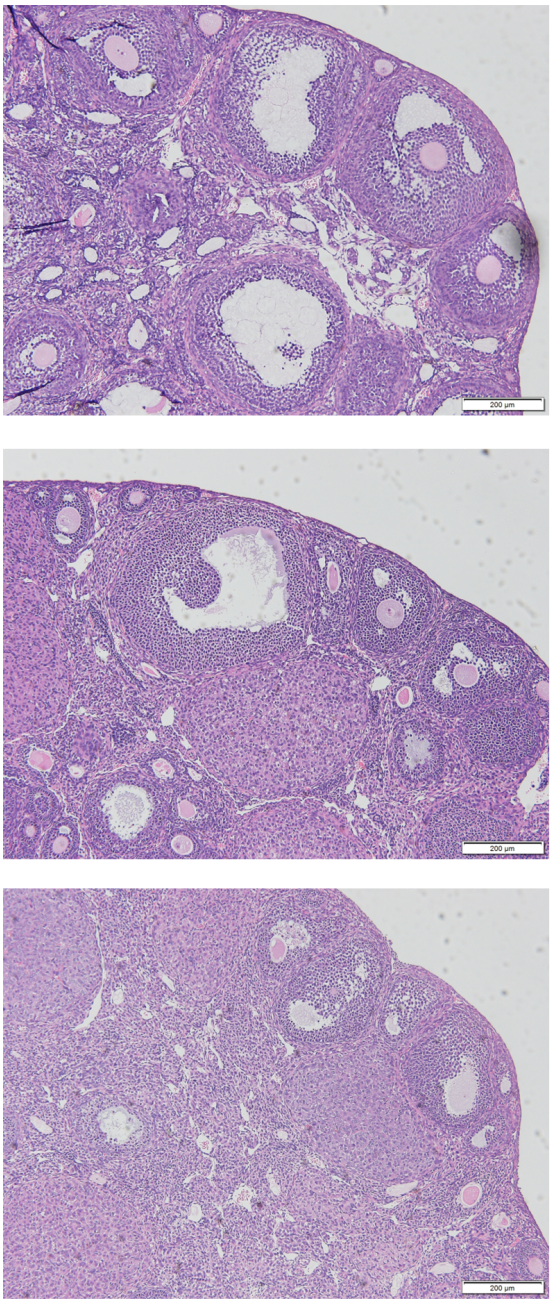

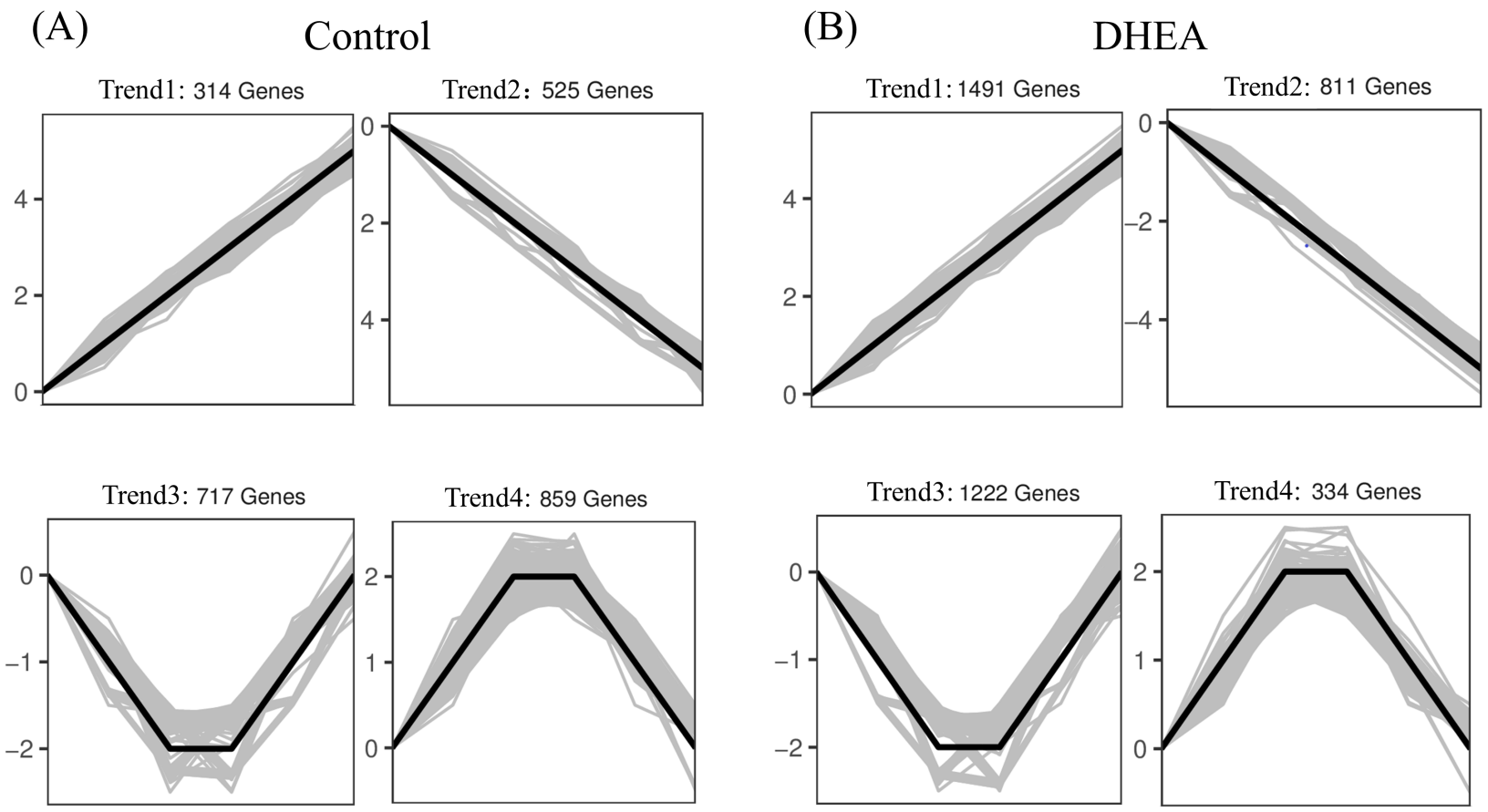
(A)
Control
Trend1: 314 Genes
Trend2: 525 Genes
Trend3: 717 Genes
Trend4: 859 Genes
(B)
DHEA
Trend1: 1491 Genes
Trend2: 811 Genes
Trend3: 1222 Genes
Trend4: 334 Genes

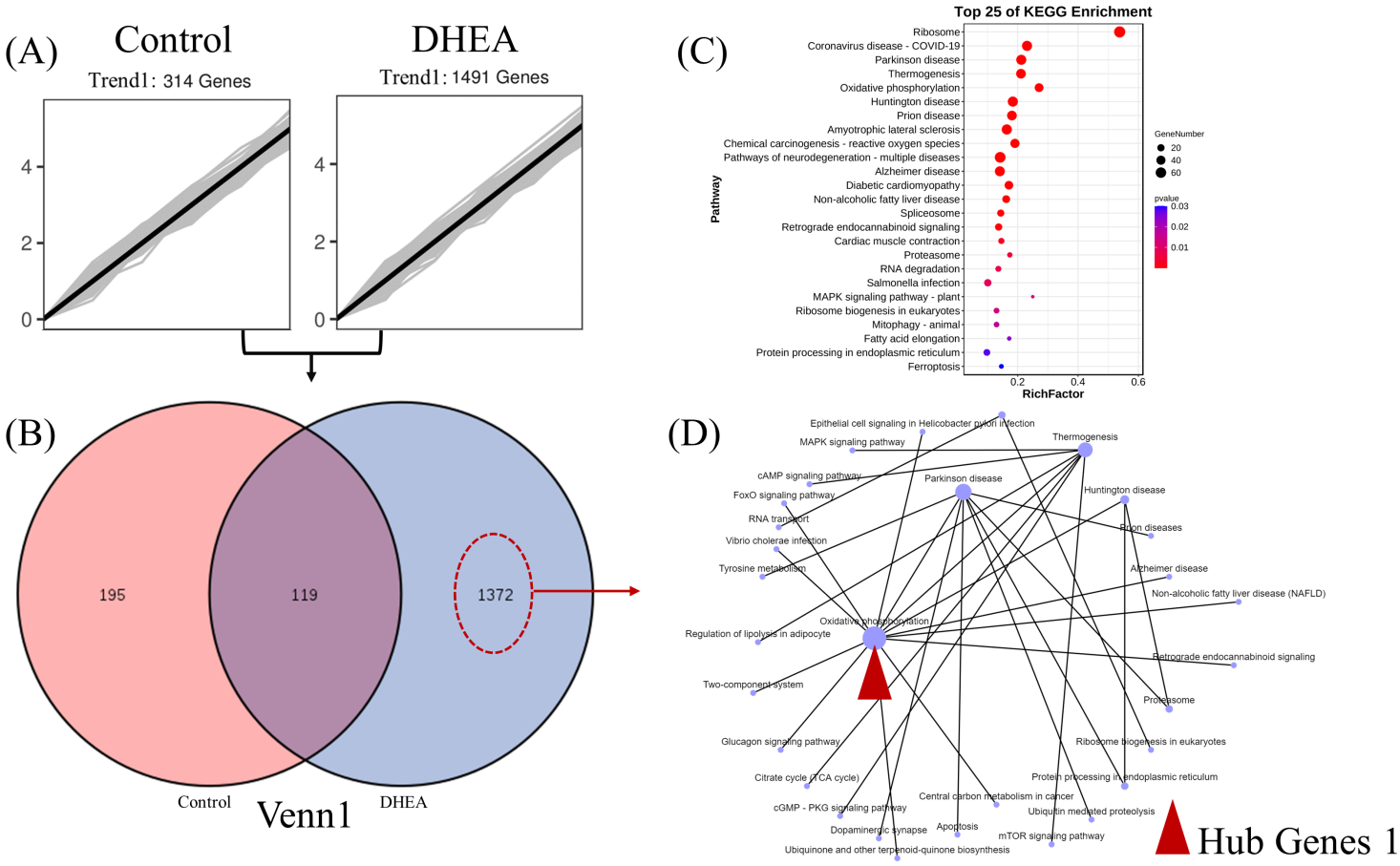
(A)
Control
Trend1: 314 Genes
DHEA
Trend1: 1491 Genes
(B)
195
119
1372
Control
DHEA
Venn1
(C)
Top 25 of KEGG Enrichment
Ribosome
Coronavirus disease - COVID-19
Parkinson disease
Thermogenesis
Oxidative phosphorylation
Huntington disease
Prion disease
Amyotrophic lateral sclerosis
Chemical carcinogenesis - reactive oxygen species
Pathways of neurodegeneration - multiple diseases
Alzheimer disease
Diabetic cardiomyopathy
Non-alcoholic fatty liver disease
Spliceosome
Retrograde endocannabinoid signaling
Cardiac muscle contraction
Proteasome
RNA degradation
Salmonella infection
MAPK signaling pathway - plant
Ribosome biogenesis in eukaryotes
Mitophagy - animal
Fatty acid elongation
Protein processing in endoplasmic reticulum
Ferroptosis
Pathway
RichFactor
GeneNumber
pvalue
(D)
Epithelial cell signaling in Helicobacter pylori infection
MAPK signaling pathway
Thermogenesis
cAMP signaling pathway
Parkinson disease
Huntington disease
FoxO signaling pathway
RNA transport
Prion diseases
Vibrio cholerae infection
Tyrosine metabolism
Alzheimer disease
Non-alcoholic fatty liver disease (NAFLD)
Oxidative phosphorylation
Regulation of lipolysis in adipocyte
Retrograde endocannabinoid signaling
Two-component system
Proteasome
Glucagon signaling pathway
Ribosome biogenesis in eukaryotes
Citrate cycle (TCA cycle)
Protein processing in endoplasmic reticulum
Central carbon metabolism in cancer
cGMP - PKG signaling pathway
Ubiquitin mediated proteolysis
Dopaminergic synapse
Apoptosis
mTOR signaling pathway
Ubiquinone and other terpenoid-quinone biosynthesis
Hub Genes 1

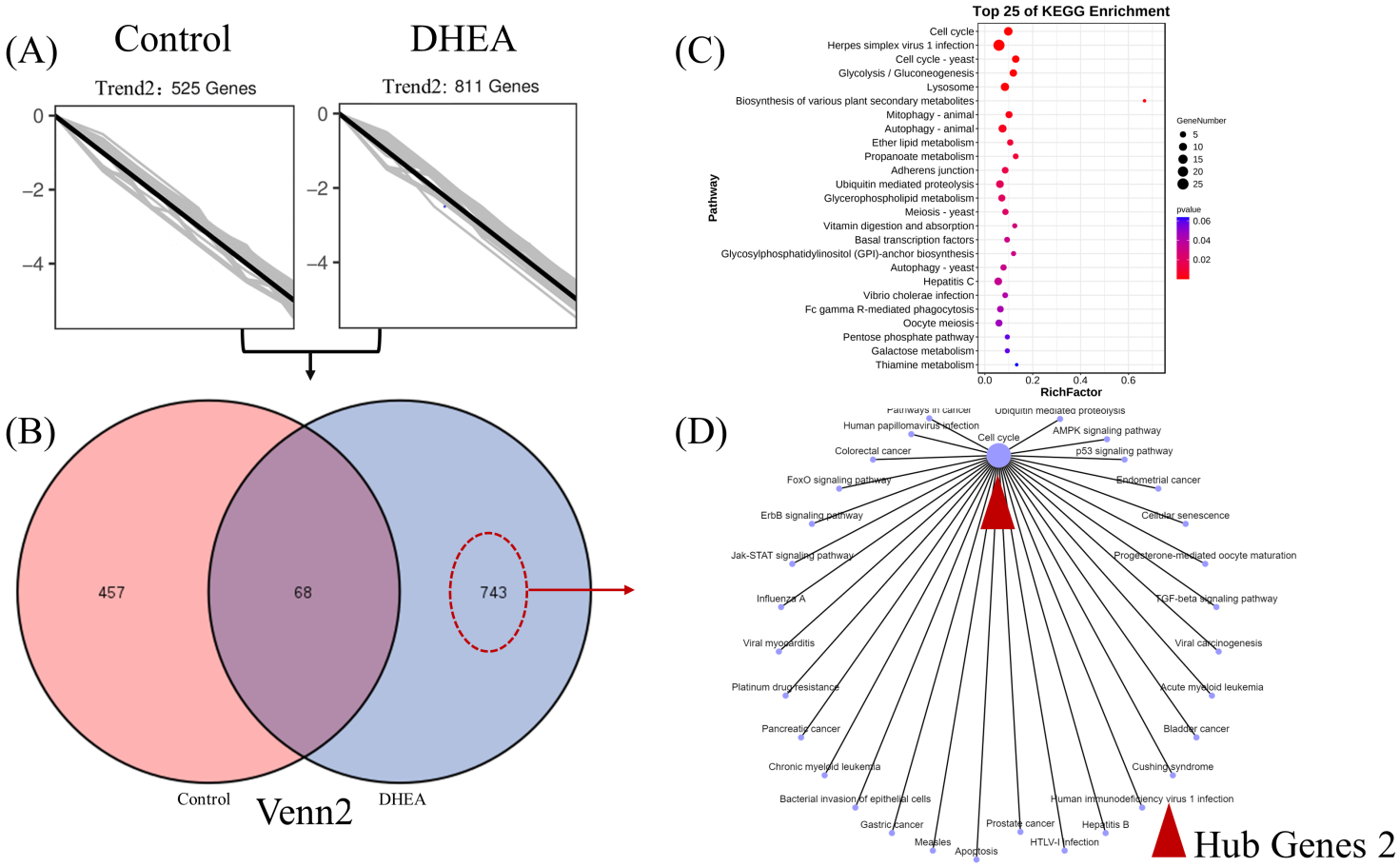
(A)
Control
DHEA
Trend2：525 Genes
Trend2: 811 Genes
0
−2
−4
(B)
457
68
743
Control
DHEA
Venn2
(C)
Top 25 of KEGG Enrichment
Pathway
RichFactor
0.0
0.2
0.4
0.6
Cell cycle
Herpes simplex virus 1 infection
Cell cycle - yeast
Glycolysis / Gluconeogenesis
Lysosome
Biosynthesis of various plant secondary metabolites
Mitophagy - animal
Autophagy - animal
Ether lipid metabolism
Propanoate metabolism
Adherens junction
Ubiquitin mediated proteolysis
Glycerophospholipid metabolism
Meiosis - yeast
Vitamin digestion and absorption
Basal transcription factors
Glycosylphosphatidylinositol (GPI)-anchor biosynthesis
Autophagy - yeast
Hepatitis C
Vibrio cholerae infection
Fc gamma R-mediated phagocytosis
Oocyte meiosis
Pentose phosphate pathway
Galactose metabolism
Thiamine metabolism
GeneNumber
5
10
15
20
25
pvalue
0.06
0.04
0.02
(D)
Pathways in cancer
Ubiquitin mediated proteolysis
Human papillomavirus infection
Cell cycle
AMPK signaling pathway
Colorectal cancer
p53 signaling pathway
FoxO signaling pathway
Endometrial cancer
ErbB signaling pathway
Cellular senescence
Jak-STAT signaling pathway
Progesterone-mediated oocyte maturation
Influenza A
TGF-beta signaling pathway
Viral myocarditis
Viral carcinogenesis
Platinum drug resistance
Acute myeloid leukemia
Pancreatic cancer
Bladder cancer
Chronic myeloid leukemia
Cushing syndrome
Bacterial invasion of epithelial cells
Human immunodeficiency virus 1 infection
Gastric cancer
Prostate cancer
Hepatitis B
Measles
HTLV-I infection
Apoptosis
Hub Genes 2

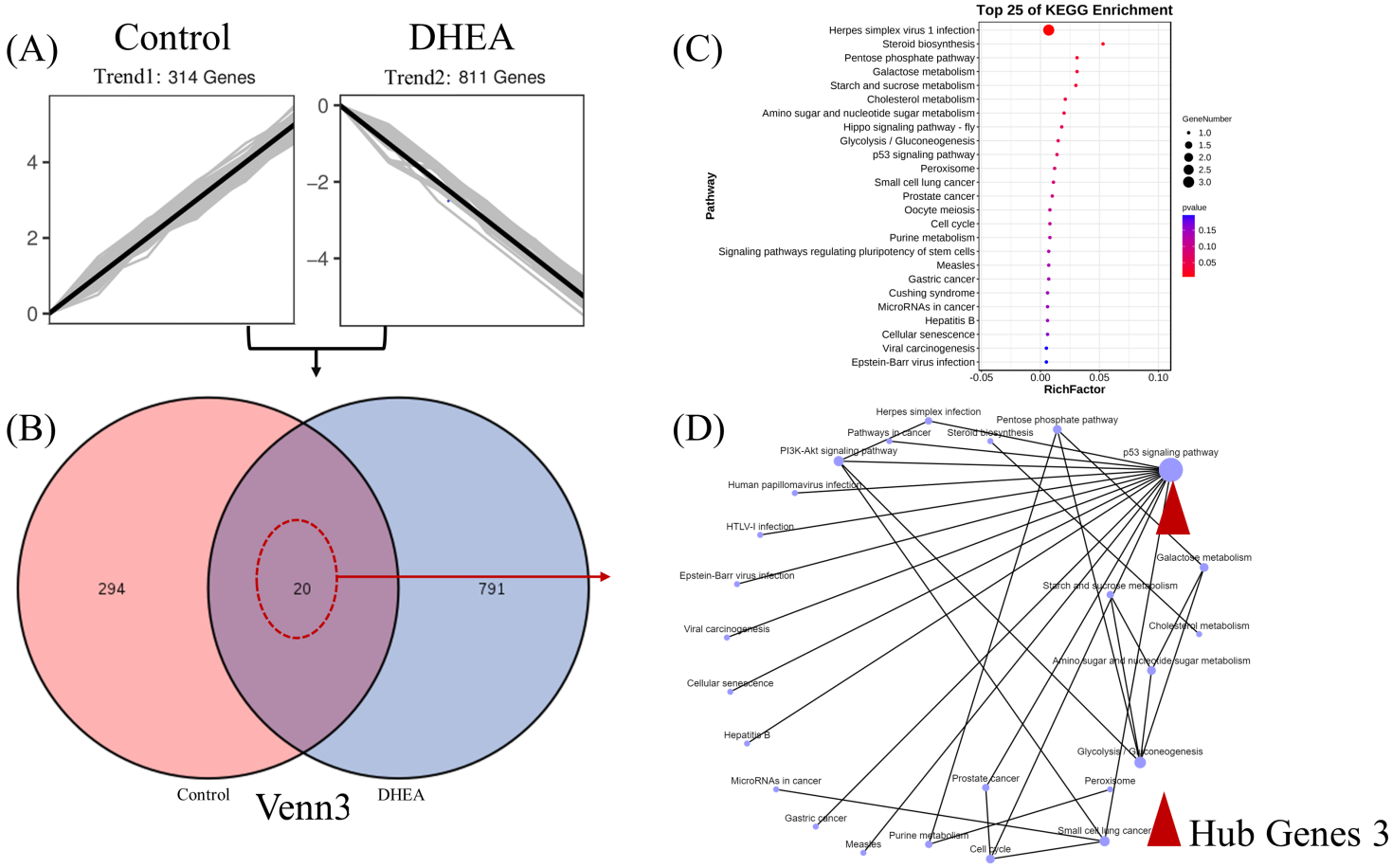
(A)
Control
Trend1: 314 Genes
DHEA
Trend2: 811 Genes
(B)
294
20
791
Control
DHEA
Venn3
(C)
Top 25 of KEGG Enrichment
Pathway
RichFactor
GeneNumber
pvalue
(D)
Hub Genes 3

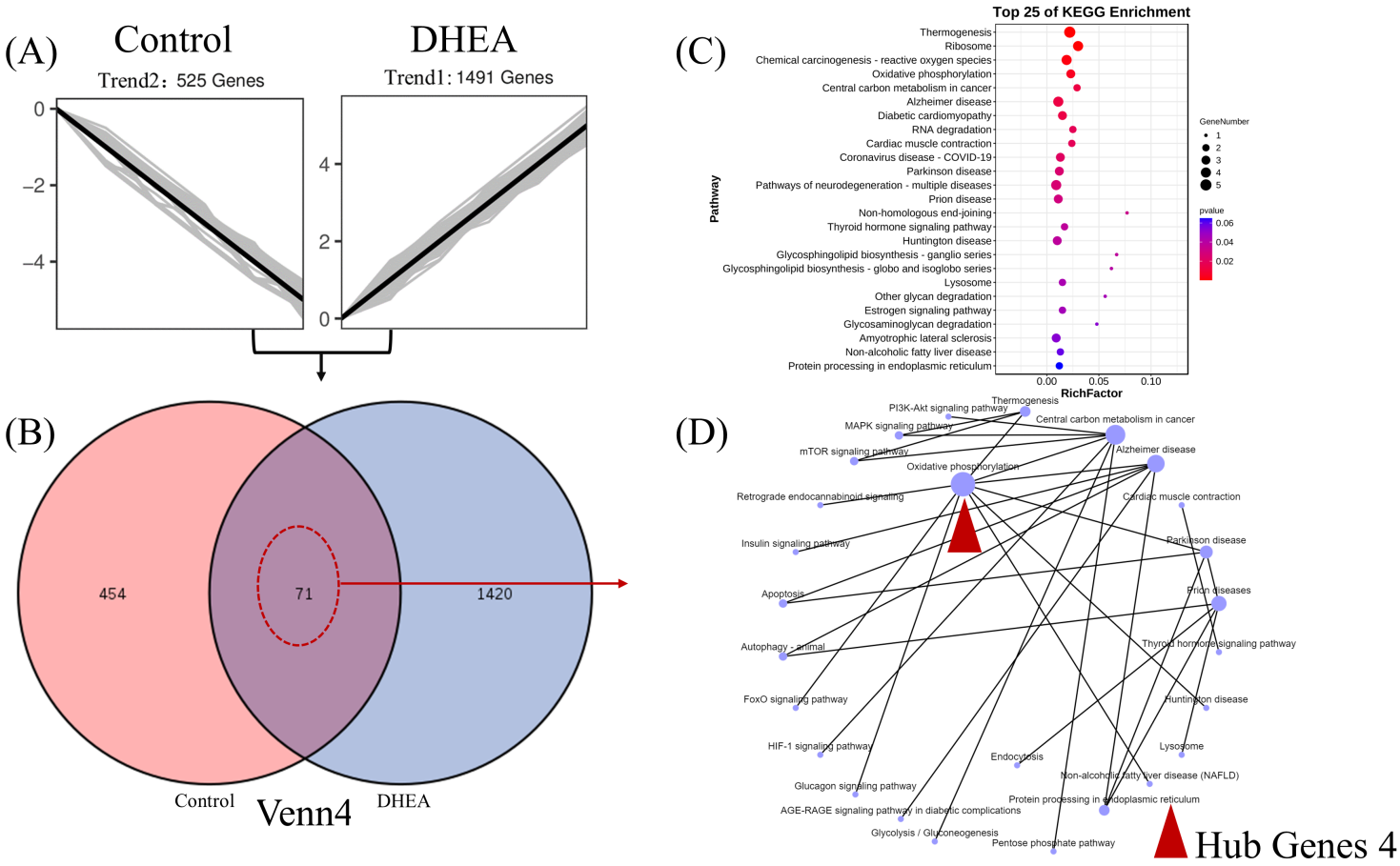
(A)
Control
DHEA
Trend2：525 Genes
Trend1：1491 Genes
(B)
454
71
1420
Control
DHEA
Venn4
(C)
Top 25 of KEGG Enrichment
Thermogenesis
Ribosome
Chemical carcinogenesis - reactive oxygen species
Oxidative phosphorylation
Central carbon metabolism in cancer
Alzheimer disease
Diabetic cardiomyopathy
RNA degradation
Cardiac muscle contraction
Coronavirus disease - COVID-19
Parkinson disease
Pathways of neurodegeneration - multiple diseases
Prion disease
Non-homologous end-joining
Thyroid hormone signaling pathway
Huntington disease
Glycosphingolipid biosynthesis - ganglio series
Glycosphingolipid biosynthesis - globo and isoglobo series
Lysosome
Other glycan degradation
Estrogen signaling pathway
Glycosaminoglycan degradation
Amyotrophic lateral sclerosis
Non-alcoholic fatty liver disease
Protein processing in endoplasmic reticulum
Pathway
RichFactor
GeneNumber
pvalue
(D)
Thermogenesis
PI3K-Akt signaling pathway
MAPK signaling pathway
mTOR signaling pathway
Central carbon metabolism in cancer
Alzheimer disease
Oxidative phosphorylation
Retrograde endocannabinoid signaling
Cardiac muscle contraction
Insulin signaling pathway
Parkinson disease
Apoptosis
Prion diseases
Autophagy - Animal
Thyroid hormone signaling pathway
FoxO signaling pathway
Huntington disease
HIF-1 signaling pathway
Endocytosis
Lysosome
Non-alcoholic fatty liver disease (NAFLD)
Glucagon signaling pathway
Protein processing in endoplasmic reticulum
AGE-RAGE signaling pathway in diabetic complications
Glycolysis / Gluconeogenesis
Pentose phosphate pathway
Hub Genes 4

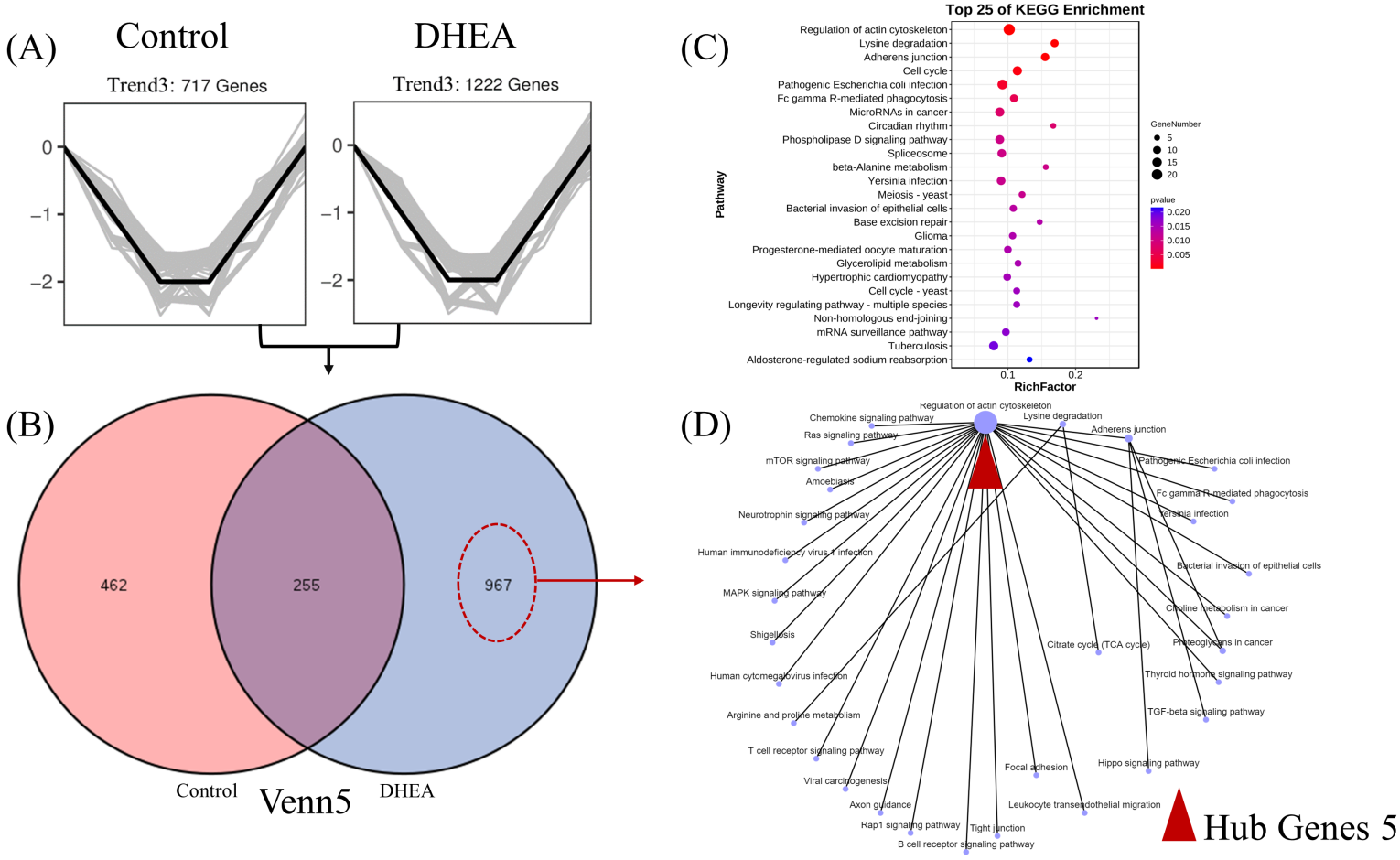
(A)
Control
DHEA
Trend3: 717 Genes
Trend3: 1222 Genes
0
−1
−2
(B)
462
255
967
Control
Venn5
DHEA
(C)
Top 25 of KEGG Enrichment
Regulation of actin cytoskeleton
Lysine degradation
Adherens junction
Cell cycle
Pathogenic Escherichia coli infection
Fc gamma R-mediated phagocytosis
MicroRNAs in cancer
Circadian rhythm
Phospholipase D signaling pathway
Spliceosome
beta-Alanine metabolism
Yersinia infection
Meiosis - yeast
Bacterial invasion of epithelial cells
Base excision repair
Glioma
Progesterone-mediated oocyte maturation
Glycerolipid metabolism
Hypertrophic cardiomyopathy
Cell cycle - yeast
Longevity regulating pathway - multiple species
Non-homologous end-joining
mRNA surveillance pathway
Tuberculosis
Aldosterone-regulated sodium reabsorption
Pathway
0.1
0.2
RichFactor
GeneNumber
5
10
15
20
pvalue
0.020
0.015
0.010
0.005
(D)
Regulation of actin cytoskeleton
Chemokine signaling pathway
Ras signaling pathway
mTOR signaling pathway
Amoebiasis
Neurotrophin signaling pathway
Human immunodeficiency virus 1 infection
MAPK signaling pathway
Shigellosis
Human cytomegalovirus infection
Arginine and proline metabolism
T cell receptor signaling pathway
Viral carcinogenesis
Axon guidance
Rap1 signaling pathway
Tight junction
B cell receptor signaling pathway
Focal adhesion
Leukocyte transendothelial migration
Lysine degradation
Adherens junction
Pathogenic Escherichia coli infection
Fc gamma R-mediated phagocytosis
Yersinia infection
Bacterial invasion of epithelial cells
Choline metabolism in cancer
Proteoglycans in cancer
Citrate cycle (TCA cycle)
Thyroid hormone signaling pathway
TGF-beta signaling pathway
Hippo signaling pathway
Hub Genes 5

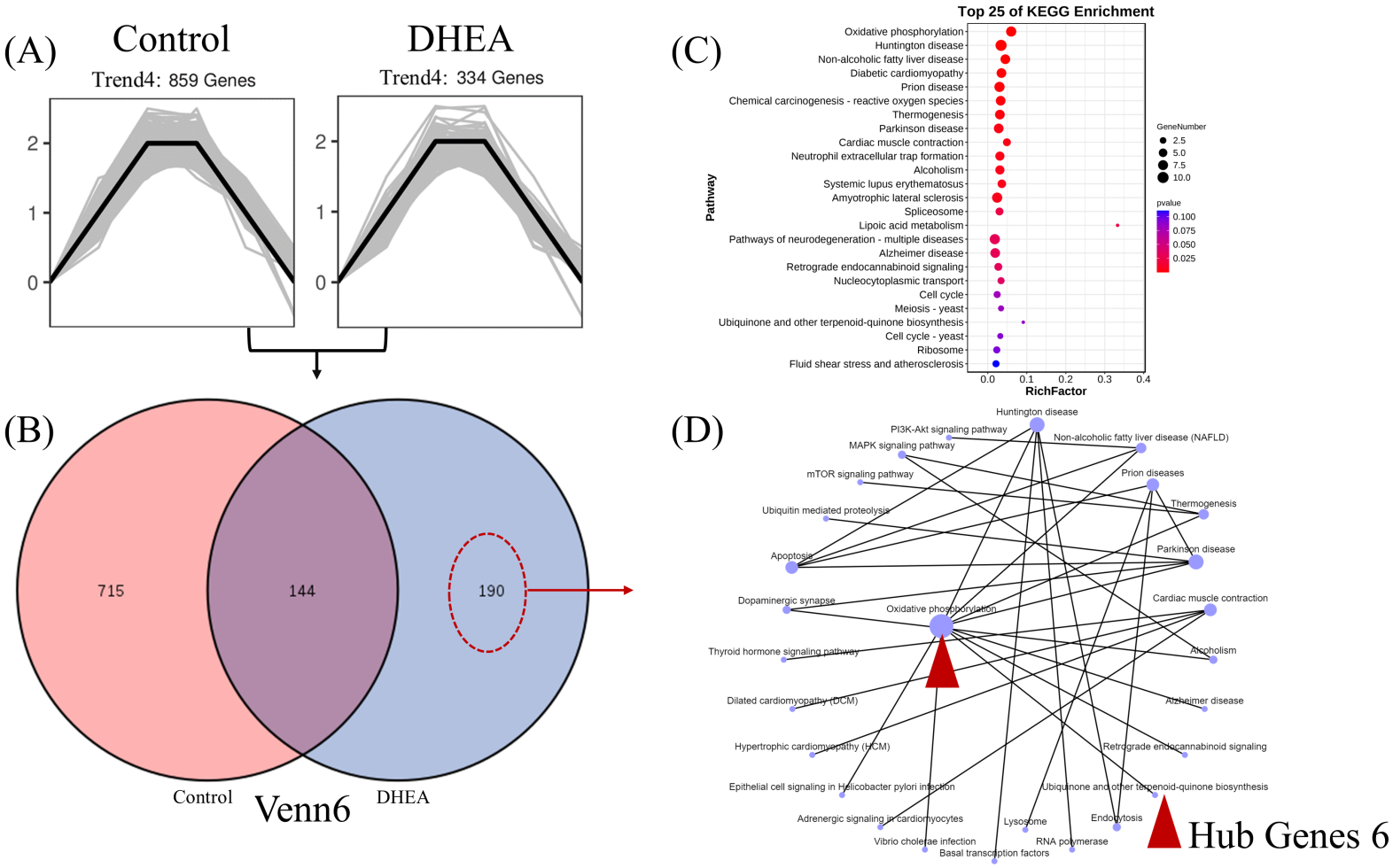
(A)
Control
Trend4: 859 Genes
DHEA
Trend4: 334 Genes
(B)
715
144
190
Control
Venn6
DHEA
(C)
Top 25 of KEGG Enrichment
Oxidative phosphorylation
Huntington disease
Non-alcoholic fatty liver disease
Diabetic cardiomyopathy
Prion disease
Chemical carcinogenesis - reactive oxygen species
Thermogenesis
Parkinson disease
Cardiac muscle contraction
Neutrophil extracellular trap formation
Alcoholism
Systemic lupus erythematosus
Amyotrophic lateral sclerosis
Spliceosome
Lipoic acid metabolism
Pathways of neurodegeneration - multiple diseases
Alzheimer disease
Retrograde endocannabinoid signaling
Nucleocytoplasmic transport
Cell cycle
Meiosis - yeast
Ubiquinone and other terpenoid-quinone biosynthesis
Cell cycle - yeast
Ribosome
Fluid shear stress and atherosclerosis
Pathway
RichFactor
GeneNumber
pvalue
(D)
Huntington disease
PI3K-Akt signaling pathway
Non-alcoholic fatty liver disease (NAFLD)
MAPK signaling pathway
mTOR signaling pathway
Prion diseases
Thermogenesis
Ubiquitin mediated proteolysis
Parkinson disease
Apoptosis
Dopaminergic synapse
Oxidative phosphorylation
Cardiac muscle contraction
Thyroid hormone signaling pathway
Alcoholism
Dilated cardiomyopathy (DCM)
Alzheimer disease
Hypertrophic cardiomyopathy (HCM)
Retrograde endocannabinoid signaling
Epithelial cell signaling in Helicobacter pylori infection
Ubiquinone and other terpenoid-quinone biosynthesis
Adrenergic signaling in cardiomyocytes
Lysosome
Endocytosis
Vibrio cholerae infection
RNA polymerase
Basal transcription factors
Hub Genes 6

Table1. Top 10 DEGs Up-regulated in DHEA injection group

	Gene ID	Gene name	Log2FC	Pvalue
DHEA injection for 1 week (Point1)	ENSMUSG00000023026	Dip2b	3.65	4.43E-37
	ENSMUSG00000071072	Ptges3	2.57	2.51E-28
	ENSMUSG00000027367	Stard7	2.43	1.70E-24
	ENSMUSG00000018363	Smurf2	2.32	6.56E-21
	ENSMUSG00000020847	Rph3al	2.20	3.55E-20
	ENSMUSG00000051579	Tceal8	2.16	6.18E-21
	ENSMUSG00000022419	Deptor	2.12	9.36E-20
	ENSMUSG00000038679	Trps1	2.09	1.15E-16
	ENSMUSG00000072889	Nfxl1	2.04	7.62E-19
	ENSMUSG00000013973	Dedd	2.03	1.87E-19
DHEA injection for 2 weeks (Point2)	ENSMUSG00000021361	Tmem14c	7.70	8.49E-130
	ENSMUSG00000034795	Ccdc122	3.43	1.30E-40
	ENSMUSG00000035506	Slc12a8	3.22	4.47E-37
	ENSMUSG00000023032	Slc4a8	2.46	1.68E-29
	ENSMUSG00000064357	mt-Atp6	1.96	1.69E-23
	ENSMUSG00000069867	Pabpn1l	1.96	2.08E-22
	ENSMUSG00000051579	Tceal8	1.82	3.76E-19
	ENSMUSG00000018102	Hist1h2bc	1.79	9.15E-17
	ENSMUSG00000037058	Paip2	1.66	3.70E-18
	ENSMUSG00000022012	Enox1	1.56	3.26E-16
DHEA injection for 3 weeks (Point3)	ENSMUSG00000018362	Kpna2	5.71	1.07E-56
	ENSMUSG00000029392	Rilpl1	5.49	7.27E-89
	ENSMUSG00000060938	Rpl26	5.16	2.48E-62
	ENSMUSG00000035295	Wdr38	4.72	7.95E-44
	ENSMUSG00000020077	Srgn	4.45	1.95E-42
	ENSMUSG00000034853	Acot11	4.33	3.39E-41
	ENSMUSG00000023965	Fbxl17	4.27	2.37E-42
	ENSMUSG00000069867	Pabpn1l	4.11	2.10E-64
	ENSMUSG00000057147	Dph6	3.79	1.34E-49
	ENSMUSG00000041453	Rpl21	3.57	8.05E-34

Table2. Top 10 DEGs Down-regulated in DHEA injection group

	Gene ID	Gene name	Log2FC	Pvalue
DHEA injection for 1 week (Point1)	ENSMUSG00000024066	Xdh	-9.12	8.27E-91
	ENSMUSG00000027871	Hsd3b1	-7.35	1.46E-79
	ENSMUSG00000021361	Tmem14c	-6.90	3.25E-109
	ENSMUSG00000060032	H2afj	-6.40	2.29E-60
	ENSMUSG00000020522	Mfap3	-3.19	5.46E-32
	ENSMUSG00000067297	Ifit1bl2	-2.41	3.05E-26
	ENSMUSG00000071226	Cecr2	-2.36	2.60E-23
	ENSMUSG00000032968	Inha	-2.12	6.05E-22
	ENSMUSG00000015837	Sqstm1	-2.03	2.14E-17
	ENSMUSG00000073705	Apitd1	-2.00	2.98E-20
DHEA injection for 2 weeks (Point2)	ENSMUSG00000032968	Inha	-4.62	3.08E-67
	ENSMUSG00000041536	Serpina3a	-4.36	6.44E-39
	ENSMUSG00000079033	Mef2b	-4.21	1.28E-43
	ENSMUSG00000055430	Nap1l5	-4.11	4.34E-43
	ENSMUSG00000063229	Ldha	-3.82	1.29E-39
	ENSMUSG00000036180	Gatad2a	-3.16	2.81E-26
	ENSMUSG00000035696	Rnf38	-3.00	1.52E-29
	ENSMUSG00000028646	Rragc	-2.97	4.31E-29
	ENSMUSG00000008348	Ubc	-2.83	1.89E-30
	ENSMUSG00000059743	Fdps	-2.64	9.96E-20
DHEA injection for 3 weeks (Point3)	ENSMUSG00000064363	mt-Nd4	-7.00	6.11E-104
	ENSMUSG00000020282	Rhbdf1	-5.87	7.83E-60
	ENSMUSG00000061371	Zfp873	-3.27	5.50E-34
	ENSMUSG00000057135	Scimp	-3.18	5.31E-32
	ENSMUSG00000076613	Ighg2b	-3.14	1.64E-31
	ENSMUSG00000021640	Naip1	-2.82	1.70E-30
	ENSMUSG00000107743	RP23	-2.46	5.97E-27
	ENSMUSG00000027834	Serpini1	-2.44	3.19E-26
	ENSMUSG00000032359	Ctsh	-2.23	1.35E-22
	ENSMUSG00000043289	Mei4	-2.22	6.96E-21

Table3. Top 10 DEGs Up-regulated in DHEA group

	Gene ID	Gene name	Log2FC	Pvalue
DHEA injection stopped for 1 week (Point4)	ENSMUSG00000018362	Kpna2	6.11	1.22E-58
	ENSMUSG00000029392	Rilpl1	4.94	2.34E-68
	ENSMUSG00000024066	Xdh	4.71	8.46E-50
	ENSMUSG00000069867	Pabpn1l	4.41	5.87E-65
	ENSMUSG00000057147	Dph6	3.76	1.27E-46
	ENSMUSG00000023026	Dip2b	3.61	3.62E-32
	ENSMUSG00000100618	Gm29595	3.31	1.22E-33
	ENSMUSG00000041840	Haus1	3.24	8.28E-37
	ENSMUSG00000035696	Rnf38	3.12	5.47E-35
	ENSMUSG00000042712	Wbp5	2.93	2.31E-26
DHEA injection stopped for 2 weeks (Point5)	ENSMUSG00000019947	Arid5b	6.52	6.00E-58
	ENSMUSG00000034324	Tmem132c	5.98	2.49E-49
	ENSMUSG00000029392	Rilpl1	5.76	2.63E-85
	ENSMUSG00000023932	Cdc5l	5.07	7.39E-49
	ENSMUSG00000032968	Inha	4.94	6.69E-60
	ENSMUSG00000041453	Rpl21	4.81	3.89E-45
	ENSMUSG00000034853	Acot11	4.67	6.39E-48
	ENSMUSG00000056116	H2-T22	4.43	1.42E-44
	ENSMUSG00000000184	Ccnd2	4.40	5.64E-38
	ENSMUSG00000020077	Srgn	3.85	4.57E-38

Table4. Top 10 DEGs Down-regulated in DHEA group

	Gene ID	Gene name	Log2FC	Pvalue
DHEA injection stopped for 1 week (Point4)	ENSMUSG00000058147	Xlr3c	-2.86	1.64E-41
	ENSMUSG00000073125	Xlr3b	-1.73	2.79E-19
	ENSMUSG00000048701	Ccdc6	-1.59	7.62E-18
	ENSMUSG00000020870	Cdc34-ps	-1.54	7.08E-16
	ENSMUSG00000068823	Csde1	-1.52	1.72E-16
	ENSMUSG00000020962	Gtf2a1	-1.49	4.29E-15
	ENSMUSG00000093930	Hmgcs1	-1.43	4.55E-15
	ENSMUSG00000071089	Trim75	-1.37	5.44E-13
	ENSMUSG00000021488	Nsd1	-1.34	1.38E-12
	ENSMUSG00000024077	Strn	-1.26	2.11E-12
DHEA injection stopped for 2 weeks (Point5)	ENSMUSG00000076613	Ighg2b	-7.01	2.71E-93
	ENSMUSG00000076615	Ighg3	-6.44	1.15E-64
	ENSMUSG00000026276	2-Sep	-5.03	6.39E-59
	ENSMUSG00000022661	Cd200	-4.77	1.73E-56
	ENSMUSG00000057135	Scimp	-4.44	6.97E-51
	ENSMUSG00000035506	Slc12a8	-4.07	5.97E-59
	ENSMUSG00000026205	Slc23a3	-3.84	2.49E-57
	ENSMUSG00000027367	Stard7	-3.43	9.48E-44
	ENSMUSG00000035455	Fignl1	-2.88	1.45E-34
	ENSMUSG00000107743	RP23	-2.77	1.50E-37

Table5. Hub genes from 6 key pathways

	Gene ID	Gene Name	Average FPKM
Hub Genes 1	ENSMUSG00000064351	mt-Co1	1081.77
	ENSMUSG00000064341	mt-Nd1	673.02
	ENSMUSG00000014294	Ndufa2	534.84
	ENSMUSG00000064354	mt-Co2	438.84
	ENSMUSG00000035885	Cox8a	363.63
	ENSMUSG00000064345	mt-Nd2	261.79
	ENSMUSG00000022354	Ndufb9	200.52
	ENSMUSG00000064368	mt-Nd6	170.56
	ENSMUSG00000031818	Cox4i1	154.07
	ENSMUSG00000044894	Uqcrq	151.30
Hub Genes 2	ENSMUSG00000036309	Skp1	2040.43
	ENSMUSG00000041431	Ccnb1	173.96
	ENSMUSG00000029012	Orc5	148.94
	ENSMUSG00000037159	Wee2	124.26
	ENSMUSG00000063065	Mapk3	93.18
	ENSMUSG00000032113	Chek1	79.23
	ENSMUSG00000006398	Cdc20	60.52
	ENSMUSG00000038482	Tfdp1	28.51
	ENSMUSG00000028587	Orc1	15.81
	ENSMUSG00000076432	Ywhaq	13.66
Hub Genes 3	ENSMUSG00000002068	Ccne1	1.86
Hub Genes 4	ENSMUSG00000064354	mt-Co2	438.84
	ENSMUSG00000044894	Uqcrq	151.30
	ENSMUSG00000064360	mt-Nd3	58.99
Hub Genes 5	ENSMUSG00000062825	Actg1	18.93
	ENSMUSG00000022021	Diap3	11.77
	ENSMUSG00000030774	Pak1	10.43
	ENSMUSG00000039936	Pik3cd	9.77
	ENSMUSG00000030265	Kras	7.79
	ENSMUSG00000025809	Itgb1	6.73
	ENSMUSG00000054808	Actn4	6.71
	ENSMUSG00000018830	Myh11	6.05
	ENSMUSG00000028868	Wasf2	5.62
	ENSMUSG00000020611	Gna13	5.18
Hub Genes 6	ENSMUSG00000022450	Ndufa6	299.40
	ENSMUSG00000024248	Cox7a2l	218.98
	ENSMUSG00000016427	Ndufa1	143.59
	ENSMUSG00000019210	Atp6v1e1	88.67
	ENSMUSG00000028648	Ndufs5	41.85
	ENSMUSG00000030785	Cox6a2	30.00

ENSMUSG00000014313	Cox6c	28.76
ENSMUSG00000024038	Ndufv3	19.49

Figure1. The schematics of the study design.

Figure2. RNA-seq data analysis flowchart.

Figure3. Ovarian histology and serum testosterone.

Figure4. Trend analysis of each group.

Figure5. Analysis of genes expressed as 'trend1' in both groups.

Figure6. Analysis of genes expressed as 'trend2' in both groups.

Figure7. Analysis of genes expressed as 'trend1' in the control group and genes expressed as 'trend2' in the DHEA group.

Figure8. Analysis of genes expressed as 'trend2' in the control group and genes expressed as 'trend1' in the DHEA group.

Figure9. Analysis of genes expressed as 'trend3' in both groups.

Figure10. Analysis of genes expressed as 'trend4' in both groups.